

# Observational Restrictions and Slow-Roll D-brane Inflation in the Special $F(\phi, T)$ Gravity

Feyzollah Younesizadeh and Davoud Kamani \*

*Department of Physics, Amirkabir University of Technology (Tehran Polytechnic)*

*P.O.Box: 15875-4413, Tehran, Iran*

*e-mails: fyounesizadeh@aut.ac.ir , kamani@aut.ac.ir*

## Abstract

We shall investigate the inflation for the D-brane model, motivated by the modified gravity  $F(\phi, T)$ . This gravity has been recently introduced in the literature. The feasibility of the D-brane inflation theory in the  $F(\phi, T)$ -gravity has been studied in conjunction with the most recent Planck data. We shall analyze the slow-roll inflation in the context of the  $F(\phi)T$ -gravity, via the D-brane model. Then, we shall calculate the inflation dynamics to obtain the scalar spectral index “ $n_s$ ” and the tensor-to-scalar ratio “ $r$ ”. Besides, we investigate the dynamics of the reheating for this model. Our model accurately covers the left-hand side of the Planck data and the D-brane inflation.

*Keywords:* Modified gravity; D-brane inflation; Slow-roll parameters; The Planck data.

---

\*Corresponding author

# 1 Introduction

The spatial flatness and the scale-invariant density perturbations suggest initial conditions during the exponential inflation, known as the visible inflation. Research on the cosmic microwave background (CMB) confirms the universe's flatness and the uniformity, which indicate an accelerated expansion in the early universe [1]-[4]. Combining the inflaton field  $\phi$  with the Einstein-Hilbert action describes this inflationary period. Thus, this preserves the original inhomogeneity that leads to the observed large-scale structures.

The slow-roll inflation is an effective mechanism in which the potential of the inflation  $V(\phi)$  drives the energy density during the inflation. The inflaton undergoes the slow-roll with a nearly constant potential. Achieving this flat potential strongly poses some challenges in the models with the particle physics basis [5], [6].

The recent data from Planck, BICEP and Keck Array [7]-[9] prefer concave inflationary potentials over convex ones. The hilltop models of the inflation usually utilize concave potentials [10]-[17]. Squaring the hilltop potential is a simple solution in the symmetry-breaking of the inflation models [11], [15]-[18]. Recent analysis favors models with the negative curvature potentials over the hybrid and large field models [19]. These models were found in the particle physics models with the symmetry breaking.

After the discovery of the  $Dp$ -branes [20], the D-brane universe, with the string theory principles, was introduced. String theory obviously identifies the dilaton field  $\phi$  as the inflaton. The inflationary scale relative to the string theory scale can clarify the lack of the fine-tuning in the e-folds of growth. The inflation may originate from other dimensions, which was suggested by the D-brane inflation. The D-brane inflation models [21]-[25] effectively utilize potentials that can be complements to the  $\alpha$ -attractors [26]-[30]. The analysis of the Planck's 2018 data prominently reveals the D-brane inflation models with the string-theoretical and phenomenological elements [31].

The power-law potentials are popular inflationary models with a single monomial potential [32], where the inflation occurs at high values of the inflaton field. Models that are inspired by the particle physics, e.g., the natural inflation [33], [34] and the periodic potentials, contain a pseudo-Nambu-Goldstone boson as the inflaton. Other models that

contain the Starobinsky  $R^2$ -inflation [35], [36] and the exponential tails [37] have been introduced via the supergravity and string theory.

The main key in the inflationary process is the development of the general relativity action through the geometric part or matter component. This has led to various modified gravities with  $f(R)$ ,  $f(T)$ ,  $f(G)$ ,  $f(R, T)$ , and so on [38] - [48]. Among the appealing modified gravities, the  $F(\phi)T$ -gravity has the non-minimal coupling of the scalar field with the trace of the energy-momentum tensor “ $T$ ” [49]. This type of coupling term is generally motivated by the quantum gravity. It provides a comprehensive description of the unified gravity with other fields [50]-[53]. One of the appeals of the  $F(\phi)T$ -gravity is that at the end of the inflation, i.e., when the inflaton is decayed, the Einstein’s gravity is naturally returned. In fact, the  $F(\phi)T$ -gravity is an extension of the  $f(R, T)$ -gravity. The latter one presents attractive results for the cosmic inflation [54], [55]. In Ref. [48] the slow-roll inflation with  $F(\phi)T = \sqrt{\kappa} \phi T$  has been studied. It revealed that the Natural, Chaotic, and Starobinsky potentials behave in better agreement with the data.

All the foregoing facts, evidences and affirmative conclusions stimulated and motivated us to adopt the  $F(\phi)T$ -gravity. At first, we apply a general functional  $F(\phi)$  and an arbitrary scalar potential  $V(\phi)$ . Afterward, special forms of the functionals  $F(\phi)$  and  $V(\phi)$  will be taken into account.

This paper is organized as follows. In Sec. 2, we shall compute inflationary effects arising from the  $F(\phi)T$  term and a general potential  $V(\phi)$ , deriving the observables and slow-roll parameters. In Sec. 3, we explore the D-brane inflation by using specific forms of  $F(\phi)$  and  $V(\phi)$ , for comparing our results with the Planck 2018 data. Additionally, we shall analyze the reheating dynamics and present relevant figures. Finally, Section 4 is devoted to the conclusions and results.

## 2 The inflation via the modified gravity $F(\phi)T$

Here, we investigate the inflation via the modified gravity that emerges from the interaction between a scalar field and the trace of the energy-momentum tensor. Thus,

we start with action [48],

$$S = \int d^4x \sqrt{-g} \left( \frac{R}{2\kappa} + \beta F(\phi) g^{\mu\nu} T_{\mu\nu} + \mathcal{L}_m \right), \quad (2.1)$$

where we apply  $\kappa = 8\pi G = 1/M_{\text{P}}^2$ , in which  $M_{\text{P}}$  is the Planck mass. The functional  $\mathcal{L}_m$  represents the matter Lagrangian, which is given as follows

$$\mathcal{L}_m = -\frac{1}{2} g^{\mu\nu} \partial_\mu \phi \partial_\nu \phi - V(\phi). \quad (2.2)$$

Besides,  $T = g^{\mu\nu} T_{\mu\nu}$  is the trace of the energy-momentum tensor, which is extracted from  $\mathcal{L}_m$ . For the canonical scalar field it is given by

$$T = g^{\mu\nu} T_{\mu\nu} = -g^{\mu\nu} \frac{2}{\sqrt{-g}} \frac{\partial(\sqrt{-g} \mathcal{L}_m)}{\partial g^{\mu\nu}} = -g^{\mu\nu} \partial_\mu \phi \partial_\nu \phi - 4V(\phi). \quad (2.3)$$

The functional  $F(\phi)$  should obviously satisfy the condition  $F(0) = 0$  to ensure that after decaying of the inflaton field  $\phi$  we receive the Einstein's theory of gravity. In this section, the functional  $F(\phi)$  and the potential  $V(\phi)$  are arbitrary. However, by adjusting the parameter “ $\beta$ ” and choosing appropriate functionals  $F(\phi)$  and  $V(\phi)$ , we can match the predictions of our inflationary model with the observations.

The variation of the action (2.1) with respect to the general metric  $g_{\mu\nu}$  defines the Einstein's equation

$$R_{\mu\nu} - \frac{1}{2} g_{\mu\nu} R = \kappa T_{\mu\nu}^{(\text{eff})}, \quad (2.4)$$

where  $T_{\mu\nu}^{(\text{eff})}$  represents the effective energy-momentum tensor, associated with the total Lagrangian  $\mathcal{L}_m^{(\text{eff})} = \beta F(\phi) T + \mathcal{L}_m$ ,

$$T_{\mu\nu}^{(\text{eff})} = \frac{-2}{\sqrt{-g}} \frac{\partial(\sqrt{-g} \mathcal{L}_m^{(\text{eff})})}{\partial g^{\mu\nu}} = T_{\mu\nu} - 2\beta F \left( T_{\mu\nu} - \frac{1}{2} T g_{\mu\nu} + \Theta_{\mu\nu} \right), \quad (2.5)$$

$$\Theta_{\mu\nu} \equiv g^{\alpha\gamma} \frac{\delta T_{\alpha\gamma}}{\delta g^{\mu\nu}} = -2T_{\mu\nu} + g_{\mu\nu} \mathcal{L}_m - 2g^{\alpha\gamma} \frac{\delta^2 \mathcal{L}_m}{\delta g^{\mu\nu} \delta g^{\alpha\gamma}}. \quad (2.6)$$

The explicit form of the symmetric tensor  $\Theta_{\mu\nu}$ , for the real scalar field, possesses the feature

$$\Theta_{\mu\nu} = -\partial_\mu \phi \partial_\nu \phi - T_{\mu\nu} = -2\partial_\mu \phi \partial_\nu \phi - g_{\mu\nu} \left( \frac{1}{2} \dot{\phi}^2 - V(\phi) \right), \quad (2.7)$$

in which we used a homogeneous inflaton field  $\phi = \phi(t)$ . In this case, the Lagrangian (2.2) reduces to

$$\mathcal{L}_m = \frac{\dot{\phi}^2}{2} - V(\phi). \quad (2.8)$$

Note that we have utilized the metric signature  $(-, +, +, +)$ . The variation of the action (2.1) with respect to  $\phi$  gives the equation of motion of this field

$$(1 + 2\beta F)\nabla_\mu\nabla^\mu\phi - (1 + 4\beta F)\frac{\partial V(\phi)}{\partial\phi} - 2\beta\frac{\partial F(\phi)}{\partial\phi}(2V - \partial_\mu\phi\partial^\mu\phi) = 0. \quad (2.9)$$

Now we employ a perfect fluid, represented by  $T_{\mu\nu}^{(\text{eff})} = \text{diag}(-\rho^{(\text{eff})}, p^{(\text{eff})}, p^{(\text{eff})}, p^{(\text{eff})})$ , where  $\rho^{(\text{eff})}$  and  $p^{(\text{eff})}$  show the effective energy density and effective pressure. Thus, these quantities obtain the following forms

$$\begin{aligned} T_{00}^{(\text{eff})} &= \rho^{(\text{eff})} = \frac{1}{2}\dot{\phi}^2(1 + 2\beta F) + (1 + 4\beta F)V, \\ T_{ij}^{(\text{eff})} &= p^{(\text{eff})}g_{ij} = \left[\frac{1}{2}\dot{\phi}^2(1 + 2\beta F) - (1 + 4\beta F)V\right]g_{ij}. \end{aligned} \quad (2.10)$$

To determine the explicit form of the equation of motion of the scalar field, we can use Eq. (2.9) and or the continuity equation  $\dot{\rho}^{(\text{eff})} + 3H(\rho^{(\text{eff})} + p^{(\text{eff})}) = 0$ , which leads to the generalized Klein-Gordon equation

$$(1 + 2\beta F)(\ddot{\phi} + 3H\dot{\phi}) + \beta F_{,\phi}\dot{\phi}^2 + (1 + 4\beta F)V_{,\phi} + 4\beta F_{,\phi}V = 0. \quad (2.11)$$

where  $V_{,\phi} = dV/d\phi$  and  $F_{,\phi} = dF/d\phi$ .

By substituting Eqs. (2.10) and also the FRW metric into the Einstein equation (2.4), the Friedmann equations can be expressed in terms of  $\rho^{(\text{eff})}$  and  $p^{(\text{eff})}$ ,

$$H^2 = \frac{\kappa\rho^{(\text{eff})}}{3} = \frac{\kappa}{3}\left[\frac{\dot{\phi}^2}{2}(1 + 2\beta F) + (1 + 4\beta F)V\right], \quad (2.12)$$

$$\frac{\ddot{a}}{a} = -\frac{\kappa}{6}(3p^{(\text{eff})} + \rho^{(\text{eff})}) = -\frac{\kappa}{3}\left[\dot{\phi}^2(1 + 2\beta F) - (1 + 4\beta F)V\right], \quad (2.13)$$

$$\dot{H} = \frac{\ddot{a}}{a} - H^2 = -\frac{\kappa}{2}\dot{\phi}^2(1 + 2\beta F). \quad (2.14)$$

Combining Eq. (2.14) with the time derivative of Eq. (2.12) we acquire another form of the modified Klein-Gordon equation

$$\ddot{\phi} + 3H\dot{\phi}(1 + 2\beta F) + \beta F_{,\phi}\dot{\phi}^2 + (1 + 4\beta F)V_{,\phi} + 4\beta F_{,\phi}V = 0. \quad (2.15)$$

We should note that one may directly extract Eq. (2.13), by substituting the FRW metric into the action (2.1). Afterward, the variation of the resultant action with respect

to the degree of freedom “ $a(t)$ ” gives the equation of motion of  $a(t)$ . However, we applied the Einstein’s equation which is equation of motion for the general metric  $g_{\mu\nu}$ .

The slow-roll approach induces the conditions  $\dot{\phi}^2 \ll V$ ,  $|\ddot{\phi}| \ll |3H\dot{\phi}|$  and  $F_{,\phi}\dot{\phi}^2 \ll H\dot{\phi}$ . Thus, in these approximations, the Friedman and the modified Klein-Gordon equations take the features

$$H^2 \simeq \frac{\kappa}{3}(1 + 4\beta F)V, \quad (2.16)$$

$$3H\dot{\phi}(1 + 2\beta F) + (1 + 4\beta F)V_{,\phi} + 4\beta F_{,\phi}V \simeq 0. \quad (2.17)$$

In this approximation, the slow-roll parameters find the forms

$$\epsilon_V \simeq \frac{1}{2\kappa(1 + 2\beta F)} \left( \frac{V_{,\phi}}{V} + \frac{4\beta F_{,\phi}}{1 + 4\beta F} \right)^2, \quad (2.18)$$

$$\eta_V \simeq \frac{1}{\kappa(1 + 2\beta F)} \left[ \frac{V_{,\phi\phi}}{V} + \frac{2\beta(3 + 4\beta F)F_{,\phi}}{(1 + 2\beta F)(1 + 4\beta F)} \frac{V_{,\phi}}{V} + \frac{4\beta(1 + 2\beta F)F_{,\phi\phi} - 8\beta^2 F_{,\phi}^2}{(1 + 2\beta F)(1 + 4\beta F)} \right]. \quad (2.19)$$

As expected, in the limit  $\beta \rightarrow 0$ , these parameters prominently reduce to  $\epsilon_E$  and  $\eta_E$ .

Another crucial factor for quantifying the inflation is the number of e-folds  $N$ . It is calculated via the equation  $\Delta N = N - N_{\text{end}} = \int_{t_{\text{end}}}^t H dt = \int_{\phi_{\text{end}}}^{\phi} (H/\dot{\phi}) d\phi$ . In which  $N$  represents the number of e-folds at the cosmological time “ $t$ ” during the inflation, while  $N_{\text{end}}$  exhibits the number of e-folds at the end of the inflation. In the slow-roll approximation  $\Delta N$  is given by

$$\Delta N = \ln [a(t_{\text{end}})/a(t)] \simeq \int_{\phi_{\text{end}}}^{\phi} \left[ \frac{\kappa V}{V_{,\phi}} + \frac{2\kappa\beta V(FV_{,\phi} - 2F_{,\phi}V)}{V_{,\phi}^2} \right] d\phi, \quad (2.20)$$

The scalar power spectrum  $A_s$  is associated with the curvature perturbations [55]. In the slow-roll approximation we receive

$$A_s = \frac{3\kappa H^2}{24\pi^2 \epsilon_V} \simeq \frac{\kappa^2(1 + 4\beta F)V}{24\pi^2 \epsilon_V}. \quad (2.21)$$

The Planck, BICEP/Keck, and other observations provide the following constraint on the amplitude  $A_s$  [31],

$$A_s = (2.10 \pm 0.03) \times 10^{-9}. \quad (2.22)$$

The scalar spectral index is given by  $n_s = 1 + \frac{d \ln A_s}{d \ln k}$ . Using Eq. (2.21) we calculate “ $n_s$ ” in terms of the slow-roll parameters  $\epsilon_V$  and  $\eta_V$ ,

$$n_s \simeq 1 + \frac{d \ln A_s}{dN} = 1 + \frac{d \ln A_s}{H dt} = 1 + \frac{\dot{\phi}}{H A_s} \frac{dA_s}{d\phi}, \quad (2.23)$$

where  $d \ln k \simeq dN$  [6]. Therefore, we obtain

$$n_s = 1 + \frac{\dot{\phi}}{H} \left[ \frac{4\beta F_{,\phi}}{1+4\beta F} + \frac{V_{,\phi}}{V} - \frac{(\epsilon_V)_{,\phi}}{\epsilon_V} \right] = 1 - 2 \left[ \epsilon_V - \frac{(\epsilon_V)_{,\phi}}{\frac{4\beta F_{,\phi}}{1+4\beta F} + \frac{V_{,\phi}}{V}} \right], \quad (2.24)$$

in which we employed Eqs. (2.16), (2.17) and the definition of  $\epsilon_V$  in Eq. (2.18). By taking into account Eq. (2.19), we receive

$$\frac{(\epsilon_V)_{,\phi}}{\frac{4\beta F_{,\phi}}{1+4\beta F} + \frac{V_{,\phi}}{V}} = \eta_V - 2\epsilon_V \quad (2.25)$$

Thus, “ $n_s$ ” takes the following feature

$$n_s \simeq 1 + 2\eta_V - 6\epsilon_V. \quad (2.26)$$

According to the production of the tensor perturbations in the inflationary period, the amplitude of the gravitational waves obtains the specific form [49],

$$A_t = \frac{2\kappa}{\pi^2} H^2 \simeq \frac{2\kappa^2(1+4\beta F)V}{3\pi^2}. \quad (2.27)$$

From Eq. (2.27) and (2.21), the relationship between the tensor-to-scalar ratio  $r = A_t/A_s$  and the slow-roll parameter  $\epsilon_V$  is given by

$$r \simeq 16\epsilon_V. \quad (2.28)$$

The Planck 2018 results [8] provide strong limits on the inflationary observables. However, the BICEP/Keck 2021 (BK18) greatly enhance the maximum value for the tensor-to-scalar ratio  $r$ . The data of the Planck satellite have restricted the tensor-to-scalar ratio “ $r$ ” at a 95% confidence level

$$r < 0.065. \quad (2.29)$$

The BICEP/Keck 2021 (BK18) [56] impose the following restriction

$$r < 0.036. \quad (2.30)$$

The preferred range for the scalar spectral index “ $n_s$ ” via the Planck+BK18 is

$$n_s = 0.964 \pm 0.004. \quad (2.31)$$

The tensor spectral index “ $n_t$ ”, based on its definition  $\frac{d \ln A_t}{dk}$ , can be rewritten as

$$n_t \simeq \frac{d \ln A_t}{dN} = \frac{\dot{\phi}}{HA_t} \frac{dA_t}{d\phi} = -\frac{1}{\kappa(1+2\beta F)} \left[ \frac{4\beta F_{,\phi} V + (1+4\beta F) V_{,\phi}}{(1+4\beta F) V} \right]^2 = -2\epsilon_V. \quad (2.32)$$

Thus, we acquire the relation  $n_t = -r/8$ . This is consistent with the results in the framework of the general relativity for a single field under the slow-roll approximation [6], [49]. Notably, since the ratio “ $r$ ” always is positive, “ $n_t$ ” possesses only negative values.

We should note that the slow-roll approximation is typically utilized in the computation of the inflationary properties. Using the slow-roll approximation for the general relativity models implies that the slow-roll parameters are modest with respect to unity. Some of these models include the scalar fields that are minimally coupled.

### 3 The D-brane inflation

The D-brane inflation models have two main aspects: a string-theoretical appearance and a phenomenological view. Both are very interesting, specially after investigating the inflationary models in the Planck 2018 data [31]. The Planck 2018  $n_s - r$  plane is shown in the figure 1.

The dark blue (light blue) region describes the  $1\sigma$  ( $2\sigma$ ) confidence level for the CMB data, obtained by the Planck 2018 and BICEP/Keck 2014. They also include the baryon oscillations (BAO) data. Meanwhile, the comparison of the predictions of inflationary models with the data in [31] is on the basis of the CMB data only, excluding the BAO. The corresponding  $1\sigma$  and  $2\sigma$  regions are shown in red. As observed in [31], the left-hand side of the  $1\sigma$  dark blue and also the red regions are covered by the two yellow lines, corresponding to the  $\alpha$ -attractors. Its predictions are corresponding to  $n_s = 1 - 2/N$ , which have been shown via two yellow lines. This investigation is usually focused on the

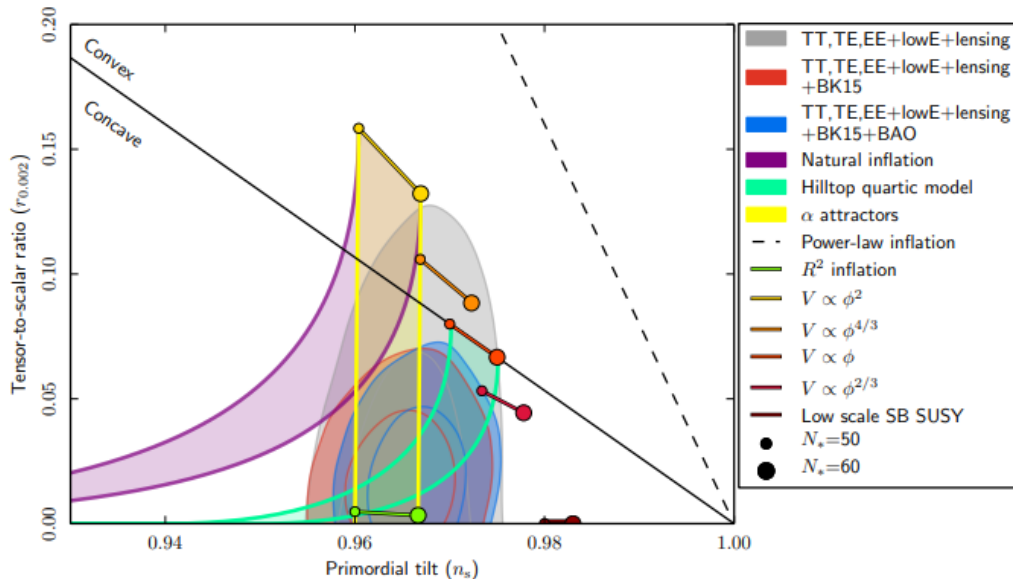


Figure 1: Using the Planck data alone (the grey area), or with the BICEP2/Keck data 2014 (red), and BAO (blue) data. The marginalized joint 68% and 95% CL areas for “ $n_s$ ” and “ $r$ ” at  $k = 0.002 Mpc^{-1}$  were compared with the theoretical predictions of specific inflationary theories. It should be noted that  $dn_s/d \ln k = 0$  is assumed in the combined 68% and 95% CL areas. The lines display the predictions of several models as a function of the number of e-folds  $N_*$ , until the end of the inflation.

configurations which contain the e-fold numbers  $N = 50$  and  $N = 60$ . The  $\alpha$ -attractor models include various inflationary models [3], [38], [57], [58].

As an example, let us simultaneously plot the predictions of the  $\alpha$ -attractors and of the simplest D-brane inflationary model with  $V \sim 1 - \left(\frac{m}{\phi}\right)^4$ . The figure 2 represents the Planck 2018 data for “ $r$ ” on  $\log_{10} r$  scale. This is more suitable for illustration of the predictions of the models in the limit of small “ $r$ ”. Both of these classes of models exhibit an attractor behavior. As one can see from this figure, the combination of the simplest  $\alpha$ -attractor model and the simplest D-brane inflation model almost completely covers the  $1\sigma$  dark blue (dark purple) area of the Planck 2018 data.

The D-brane inflation model after the Planck 2018 has phenomenologically acquired a new significance. The string theory origin of the D-brane inflation model is often attributed to the model in [21], in which the  $(\overline{D3}\text{-brane})\text{-(D3-brane)}$  interaction has been studied. Predictions of this model completely cover the right-hand side of the  $1\sigma$  dark

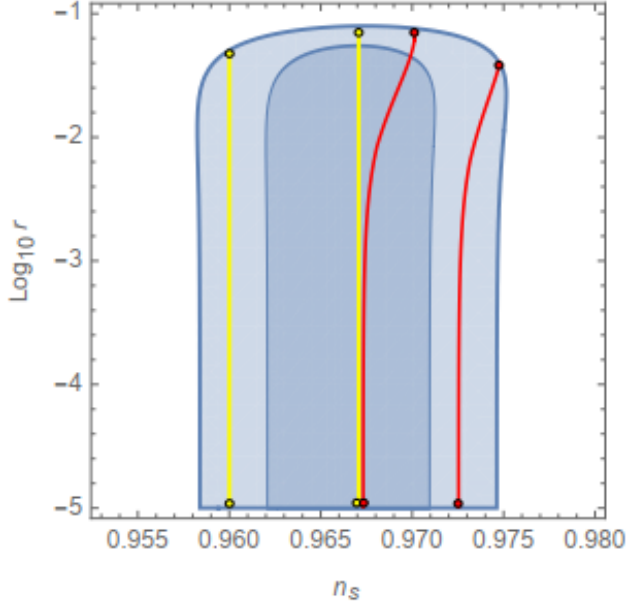


Figure 2: The Planck 2018 results [8] for “ $n_s$ ” and “ $r$ ” have been compared with the predictions of the simplest D-brane inflationary model with  $V \sim 1 - (\frac{m}{\phi})^4$  and the  $\alpha$ -attractors in the  $2\sigma$  region. The dark (light) blue region on the panel represents the Planck 2018  $1\sigma$  ( $2\sigma$ ) region. The data are related to the CMB. On the panel, the quadratic  $T$ -model of the  $\alpha$ -attractors at  $N = 50$  and  $N = 60$  has been represented by the two yellow lines. Besides, the simplest D-brane inflation model has been represented by the two red lines.

blue and also dark red areas in figure 1. The inflationary potentials, corresponding to the  $(\overline{D3}$ -brane)-(D3-brane) interaction, have been proposed as in the following forms

$$V_{\text{BI}} = V_0 \left[ 1 - \left( \frac{m}{\phi} \right)^{7-p} + \dots \right], \quad (3.1)$$

$$V_{\text{KKLTI}} = V_0 \left[ 1 + \left( \frac{m}{\phi} \right)^{7-p} \right]^{-1}, \quad (3.2)$$

where BI (KKLTI) represents the Brane Inflation (KKLT Inflation). In [16] a cosmological analysis of these potentials has been performed, with emphasis on the D3- and D5-branes. A consistent cosmological evolution of the D3-branes in the string theory, with the 10-dimensional geometry, can be interpreted as an evolution in the 4-dimensional spacetime under the condition that the 6-dimensional internal space possesses a constant volume.

In accordance with the above explanation the D3-brane model can be defined via the following potential

$$V(\phi) = V_0 \left( 1 - \frac{m^4}{\phi^4} \right). \quad (3.3)$$

Here we eliminated the higher-order terms which represent additional stabilizing terms. They are unimportant during the inflation. In other words, they become significant only after the inflaton.

Our suggested functional  $F(\phi)$  is as follows

$$F(\phi) = \frac{\phi^5}{\mu} \left( 1 - \frac{m^4}{\phi^4} \right). \quad (3.4)$$

This form of  $F(\phi)$  incorporates a non-minimal interaction between the gravity and matter. In fact, we have extended the functional  $F(\phi)$ , which was initially expressed as  $F(\phi) \sim \phi$  in [48]. However, for  $\phi^2 \ll m^2$  the functional  $F(\phi)$  is approximately proportional to  $\phi$ . As  $\phi$  tends to zero, this choice of  $F(\phi)$  obviously leads to the Einstein's theory of gravity, i.e.  $F(0) = 0$ .

More detail for the theoretical justification of the forms of  $V(\phi)$  and  $F(\phi)$ , via the physical and string-theoretic motivations, is given by the following descriptions.

### 1. Justification for the potential form

This potential can be motivated from the several perspectives:

- In the D-brane inflation models, the inflaton  $\phi$  often represents the separation in a higher-dimensional space between a D-brane and an anti-D-brane (or another D-brane). They have an attractive potential that resembles Coulomb's form [21]:

$$V(\phi) = V_0 \left( 1 - \frac{C}{\phi^n} \right), \quad (3.5)$$

where  $C$  is a constant, associated with the D-brane tension and couplings, and “ $n$ ” is dependent on the dimensions of the interacting D-branes and the compactified space. The leading-order interaction for the D3-branes in the 10-dimensional Type IIB string theory is proportional to  $1/\phi^4$ , which supports our selection of  $n = 4$ .

- The Moduli Stabilization Effects: The  $m^4$ -term may be extracted from the non-perturbative effects that stabilize the moduli fields, such as the gaugino condensation or the instanton corrections. These introduce a little correction to the flat potential at large  $\phi$  [59].

- Comparison with the Plateau Potentials: Such potentials are favored by the Planck data, because they produce sufficient inflation while keeping “ $r$ ” small, which is consistent with the observations.

## 2. Justification for the form of $F(\phi)$

The functional  $F(\phi)$  that we have used, generalizes the linear case  $F(\phi) = \phi$ . It includes the higher-order of  $\phi$ , introduced by the higher-order modifications to the effective string actions. This form of  $F(\phi)$  preserves the same symmetry and dimensional structure of the potential. It was designed to reflect the shape of the tachyon potential, which is compatible with the brane collapse scenarios.

- **The stringy Non-minimal Coupling:** In the string theory, non-minimal couplings between the scalars (like the dilaton or moduli) and the matter (encoded in  $T$ ) are common. The  $\phi^5$ -term could arise from the higher-derivative corrections (e.g.,  $\alpha'$  corrections in the string effective actions) [60].

- The factor  $(1 - \frac{m^4}{\phi^4})$  ensures the regular behavior near a specific cut-off scale (the brane separation or resolution radius), which is commonly used to mimic the stringy corrections or the moduli stabilization effects in the UV.

- **The UV-Completion and cut-off Scale  $\mu$ :** The parameter  $\mu$  acts as a cut-off scale, suppressing the higher-dimensional operators. This is natural in the effective field theories, derived from the string compactifications. Thus,  $\mu$  could be related to the string scale  $M_s$  or the Kaluza-Klein scale.

- **Matching to the Linear Limit:** For  $\phi \gg m$ , we obtain  $F(\phi) \approx \phi^5/\mu$ , but if we tune  $\mu \sim \phi^4$  (or take into account a regime in which  $\phi$  is small), it simplifies to  $F(\phi) \sim \phi$ . Hence, it reduces to the simpler form [48]. This ensures consistency with the earlier studies.

## 3. Theoretical Consistency and the Effective Field Theory Validity

- The model ensures that the corrections are perturbative by assuming  $\phi \gg m$  during inflation.

- Since  $T$  (the trace of the stress-energy tensor) is a scalar under the diffeomorphisms, and the coupling respects the general covariance, the coupling term  $F(\phi)T$  is consistent with the effective field theory principles.

Consequently, the D-brane inflation in the string theory, where the inflaton reflects the branes separation and the potential results from the brane-antibrane interactions (mostly  $\propto 1/\phi^4$  for the D3-branes), serves as the motivation for the forms of  $V(\phi)$  and

$F(\phi)$ . Using  $\phi^5/\mu$  to capture the higher-order stringy corrections and  $\mu$  as a UV cut-off, the coupling term  $F(\phi)T$  generalizes minimal couplings, looked at in the previous work. The stabilization effects of the moduli are encoded by the  $m^4/\phi^4$  term. These choices guarantee the Planck data compatibility while extending the simpler models [61].

#### 4. Motivation for the Specific Choice of $f(\phi, T)$

The scalar field  $\phi$  is coupled to the trace of the energy-momentum tensor  $T$  in the  $f(\phi, T)$  framework, which generalizes the scalar-tensor theories. This coupling term is inspired by the following criteria.

- Dynamics of the D-branes: In the string theory, the metric and the scalar field (such as the inflaton) are coupled to the D-branes. The D-brane action in a warped throat geometry naturally gives rise to the expression  $F(\phi)T$ .

- Modified gravity:  $F(\phi)T$  includes a direct interaction between the inflaton and the matter/radiation sectors, which can change the dynamics of the inflation and reheating, in contrast to the pure  $f(R)$  or the Brans-Dicke theories.

- Connection to the Conformal Invariance:

The specific form  $F(\phi) = \frac{\phi^5}{\mu} \left(1 - \frac{m^4}{\phi^4}\right)$  has been chosen because it reduces to  $F(\phi) \sim \phi$  (a common conformally invariant coupling) in the limit  $\phi \gg m$ , which links it to the well-studied models.

- The correction term  $(1 - \frac{m^4}{\phi^4})$  and the deviation from linearity, i.e.  $(\phi^5)$ , are driven by the D-brane potentials in the flux compactifications (e.g., KKLT scenarios) [62], where the inflaton potential is corrected by the non-perturbative effects or the supersymmetry breaking.

#### 5. Connection Between the D-brane Inflation and $f(\phi, T)$ Theory

In the D-brane inflation, the inflaton  $\phi$  represents the position of a D-brane in a warped throat (e.g., the Klebanov-Strassler throat) [63]. The brane's motion is governed by a scalar potential  $V(\phi)$  (e.g., from the anti-D-brane tension or the flux-induced terms). Couplings to the bulk energy-momentum tensor  $T$ , arise from the brane's interaction with the bulk fields (e.g., via the DBI action) [20]. This interaction is encoded by the  $f(\phi, T)$ -term; the brane's movement causes the perturbations to the matter fields and the bulk geometry. This results in a  $T$ -dependent correction to the 4-dimensional effective action.

Our  $F(\phi)$  is obtained from the warp-factor dependency and the non-canonical kinetic terms of the D-brane action.

By substituting the functionals (3.3) and (3.4) into Eqs. (2.18) and (2.19), the slow-roll parameters find the features

$$\epsilon_V \simeq - \frac{8\mu (3\beta m^8\phi + 2\beta m^4\phi^5 - 5\beta\phi^9 - m^4\mu)^2}{\kappa\phi^2 (m^4 - \phi^4)^2 (4\beta m^4\phi - 4\beta\phi^5 - \mu)^2 (2\beta m^4\phi - 2\beta\phi^5 - \mu)}, \quad (3.6)$$

$$\begin{aligned} \eta_V &\simeq - \frac{1}{\kappa\phi^2 (m^4 - \phi^4) (4\beta m^4\phi - 4\beta\phi^5 - \mu) (2\beta m^4\phi - 2\beta\phi^5 - \mu)^2} \\ &\times 4\mu \left( 30\beta^2 m^{12}\phi^2 - 50\beta^2 m^8\phi^6 + 10\beta^2 m^4\phi^{10} + 10\beta^2\phi^{14} - 24\beta m^8\mu\phi \right. \\ &\left. + 20\beta m^4\mu\phi^5 - 20\beta\mu\phi^9 + 5m^4\mu^2 \right). \end{aligned} \quad (3.7)$$

The quantities “ $r$ ” and “ $n_s$ ” can be expressed in terms of the parameters “ $\mu$ ”, “ $\beta$ ” and “ $m$ ” and the inflaton field  $\phi$ ,

$$r = \frac{8}{\kappa \left[ 1 + \frac{2\beta\phi^5(1-\frac{m^4}{\phi^4})}{\mu} \right]} \left( \frac{4m^4}{\phi^5 \left( 1 - \frac{m^4}{\phi^4} \right)} + \frac{\frac{4\beta}{\mu} \left[ 5\phi^4 \left( 1 - \frac{m^4}{\phi^4} \right) + 4m^4 \right]}{1 + \frac{4\beta\phi^5(1-\frac{m^4}{\phi^4})}{\mu}} \right)^2, \quad (3.8)$$

$$\begin{aligned} n_s &= 1 + \frac{8}{\kappa \left[ 1 + \frac{2\beta\phi^5(1-\frac{m^4}{\phi^4})}{\mu} \right]} \\ &\times \left\{ - \frac{5m^4}{\phi^6 \left( 1 - \frac{m^4}{\phi^4} \right)} + \frac{\frac{2\beta m^4}{\mu} \left[ 3 + 4\frac{\beta\phi^5}{\mu} \left( 1 - \frac{m^4}{\phi^4} \right) \right] \left[ 5\phi^4 \left( 1 - \frac{m^4}{\phi^4} \right) + 4m^4 \right]}{\left( 1 - \frac{m^4}{\phi^4} \right) \left[ 1 + 4\frac{\beta\phi^5}{\mu} \left( 1 - \frac{m^4}{\phi^4} \right) \right] \left[ 1 + 2\frac{\beta\phi^5}{\mu} \left( 1 - \frac{m^4}{\phi^4} \right) \right]} \phi^5 \right. \\ &+ \frac{\frac{20\beta}{\mu} \left[ 1 + 2\frac{\beta\phi^5}{\mu} \left( 1 - \frac{m^4}{\phi^4} \right) \right] \left[ \phi^3 \left( 1 - \frac{m^4}{\phi^4} \right) + \frac{m^4}{\phi} \right] - 2\frac{\beta^2}{\mu^2} \left[ 5\phi^4 \left( 1 - \frac{m^4}{\phi^4} \right) + 4m^4 \right]^2}{\left[ 1 + 4\frac{\beta\phi^5}{\mu} \left( 1 - \frac{m^4}{\phi^4} \right) \right] \left[ 1 + 2\frac{\beta\phi^5}{\mu} \left( 1 - \frac{m^4}{\phi^4} \right) \right]} \\ &\left. - 6 \left[ \frac{m^4}{\phi^5 \left( 1 - \frac{m^4}{\phi^4} \right)} + \frac{\frac{\beta}{\mu} \left[ 5\phi^4 \left( 1 - \frac{m^4}{\phi^4} \right) + 4m^4 \right]}{1 + 4\frac{\beta\phi^5}{\mu} \left( 1 - \frac{m^4}{\phi^4} \right)} \right]^2 \right\}. \end{aligned} \quad (3.9)$$

The  $\phi$  represents the field value at the time of horizon crossing, which is determined numerically from Eq. (2.20). The value  $\phi_{\text{end}}$  is specified by either  $\epsilon_V = 1$  or  $\eta_V = 1$ .

In this case,  $N$  is fixed at 50 or 60 e-folds. By adjusting appropriate values for the parameters, it is feasible to receive any desirable values for “ $n_s$ ” and “ $r$ ”.

We have employed a modified gravity model that not only aligns with the predictions on the right-hand side of the Planck data but also extends to encompass the left-hand side too. In the case of  $\beta = -0.008$  and  $m = 0.1$ , the value of “ $\mu$ ” should tend towards higher numbers. Its range may begin at  $\mu = 30$  and can extend to  $\mu = 200$  or higher. Within this range, there are  $50 \leq N \leq 60$ . In this case, we can cover the left-hand side of the Planck data. With  $\beta = -0.001$  and  $m = 0.1$ , we receive the values of “ $r$ ” and “ $n_s$ ” in the ranges  $r = [23 \times 10^{-6}, 39 \times 10^{-6}]$  and  $n_s = [0.9517, 0.9639]$  in which  $5 \leq \mu \leq 30$ . Thus, the left-hand side of the Planck data for  $N = 50$  is effectively covered.

Now consider the table 1.

Table 1: The tensor-to-scalar ratio “ $r$ ” and the scalar spectral index “ $n_s$ ” have been numerically calculated for  $N = 50 \rightarrow 60$ , with  $m = 0.08$ ,  $\beta = -0.004$  and varying  $\mu$ .

$N$	$\mu$	$n_s$	$r$
50→60	15	0.9537→0.9583	0.000019→0.000011
50→60	20	0.9567→0.9615	0.000022→0.000014
50→60	25	0.9586→0.9635	0.000024→0.000016
50→60	30	0.9599→0.9649	0.000025→0.000017
50→60	35	0.9608→0.9659	0.000026→0.000018
50→60	40	0.9615→0.9666	0.000027→0.000018
50→60	45	0.9621→0.9672	0.000027→0.000019
50→60	50	0.9625→0.9677	0.000028→0.000019

Beside this table, choosing  $1 \leq \mu \leq 5$ ,  $\beta = -0.004$  and  $m = 0.02$  allows us to effectively cover the left-hand side of the Planck data. In this case, for  $N = 50$  the values of “ $r$ ” and “ $n_s$ ” belong to the intervals  $[3 \times 10^{-6}, 4 \times 10^{-6}]$  and  $[0.9544, 0.9640]$ , respectively. In the same way, for  $N = 60$  there are  $r \in [10^{-6}, 3 \times 10^{-6}]$  and  $n_s \in [0.9591, 0.9693]$ .

Now look at the table 2.

In addition to the above table, the choices  $3 \leq \mu \leq 100$ ,  $\beta = -0.001$  and  $m = 0.08$  cover the left-hand side of the Planck data. Consequently, for  $N = 50$ , we obtain  $r \in [16 \times 10^{-6}, 31 \times 10^{-6}]$  and  $n_s \in [0.9507, 0.9661]$ . For the case  $N = 60$ , we receive  $r \in [9 \times 10^{-6}, 23 \times 10^{-6}]$  and  $n_s \in [0.9552, 0.9716]$ . The D-brane inflation with a single-field model in the Einstein’s gravity incorporates the red region of the Planck/BICEP/Keck data. Appropriate values of the parameters “ $\beta$ ”, “ $\mu$ ” and “ $m$ ” enabled us to encompass the region in the  $(n_s, r)$ -space that was preferred by the Planck 2018.

Now consider the figure 3.

Table 2: The tensor-to-scalar ratio “ $r$ ” and the scalar spectral index “ $n_s$ ” have been numerically calculated for  $N = 50 \rightarrow 60$ , with  $m = 0.3$ ,  $\beta = -0.0001$  and varying  $\mu$ .

$N$	$\mu$	$n_s$	$r$
50→60	7	0.9567→0.9615	0.000128→0.000082
50→60	9	0.9588→0.9637	0.000140→0.000093
50→60	11	0.9602→0.9652	0.000148→0.000101
50→60	13	0.9611→0.9662	0.000154→0.000106
50→60	15	0.9618→0.9670	0.000158→0.000107
50→60	17	0.9624→0.9676	0.000162→0.000113
50→60	19	0.9628→0.9680	0.000164→0.000116
50→60	21	0.9632→0.9684	0.000166→0.000118

According to this figure, which is inferred from the calculations, we can conclude that by choosing appropriate values for the parameters in the D-brane inflation, we can cover the left-hand side of the Planck data in the  $(n_s, r)$ -plane. Other suitable data enable us to cover the right-hand side of the data, like the Einstein’s gravity. Finally, we have reexamined our model predictions for the tensor-to-scalar ratio in the light of the recent observational updates from the BICEP/Keck 2021 experiment. We find that the values that we obtained for  $r$  and  $n_s$  are consistent not only with the Planck 2018 data, which include these constraints, but also with the  $r < 0.036$  (95% $CL$ ) bound in the BICEP/Keck 2021 (BK18) data. This indicates that our model is consistent with the observations for a wide range of the initial conditions and the parameter choices.

- **Reheating Dynamics in the Modified Gravity**

Next, we shall examine the reheating and its corresponding dynamics. The oscillation of the inflaton field  $\phi$  around its minimum occurs after the end of the inflation. The decay rate  $\Gamma_\phi$  indicates that the energy is transferred into the radiation through the decay. The equations for the evolution of the radiation energy density and the inflaton energy density

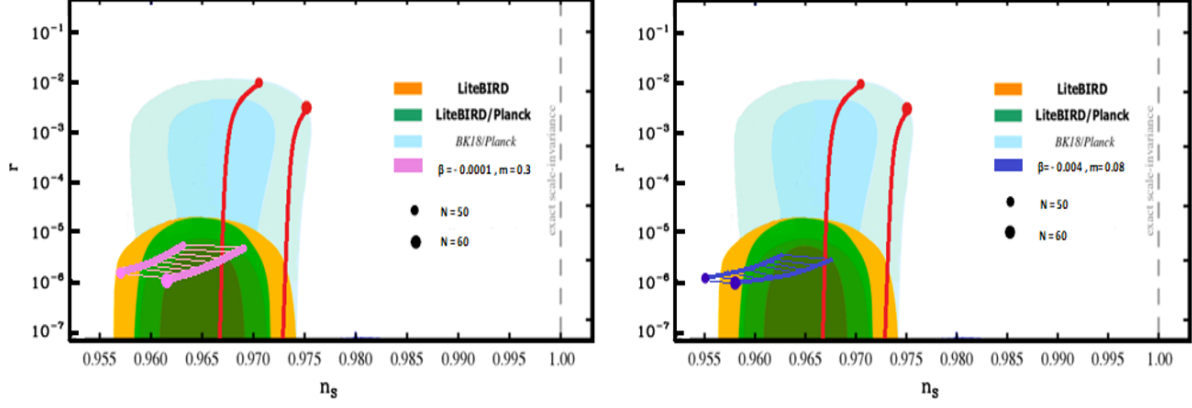


Figure 3: The predicted “ $r$ ” and “ $n_s$ ” in our model. To compare, the outcome of the Einstein’s gravity (indicated by the red bar) has been displayed, which corresponds to the D-brane inflationary model with  $V \sim 1 - \frac{m^4}{\phi^4}$ . The blue color is assigned when  $\beta = -0.004$ ,  $m = 0.08$  and  $15 \leq \mu \leq 50$ , while the pink color is assigned when  $\beta = -0.0001$ ,  $m = 0.3$  and  $7 \leq \mu \leq 21$ . At  $k = 0.002 Mpc^{-1}$ , “ $r$ ” and “ $n_s$ ” are characterized by the confidence level margins, depicted in the dark (light) blue, corresponding to the  $1\sigma$  ( $2\sigma$ ) regions, respectively. The 2018 Planck data [8] encompasses the related data to the Einstein’s gravity.

are as follows

$$\begin{aligned} \dot{\rho}_\phi + 3H(1 + \omega_\phi)\rho_\phi &= -\Gamma_\phi\rho_\phi, \\ \dot{\rho}_r + 4H\rho_r &= \Gamma_\phi\rho_\phi, \end{aligned} \quad (3.10)$$

where  $\omega_\phi$  is the effective equation of state during the oscillations, often it vanishes for the quadratic-like oscillations, which gives

$$H_{\text{reh}} \sim \Gamma_\phi. \quad (3.11)$$

Due to the modifications, at reheating we have

$$\rho_{\text{total}} = \frac{3}{\kappa} \frac{H^2}{1 + 4\beta F(\phi_{\text{reh}})}. \quad (3.12)$$

The universe thermalizes with a radiation bath at the moment when  $H \sim \Gamma_\phi$ ,

$$\rho_r = \frac{\pi^2}{30} g_* T_{\text{reh}}^4, \quad (3.13)$$

and

$$\rho_r \approx \frac{3}{\kappa} \frac{\Gamma_\phi^2}{1 + 4\beta F(\phi_{\text{reh}})}. \quad (3.14)$$

Thus, the temperature at the end of reheating is defined as follows

$$T_{\text{reh}} = \left( \frac{90}{\pi^2 g_* \kappa} \frac{\Gamma_\phi^2}{1 + 4\beta F(\phi_{\text{reh}})} \right)^{1/4}, \quad (3.15)$$

where  $g_*$  is an effective relativistic degree of freedom, and its typical value is  $g_* \sim 100$ . Near the minimum of the potential ( $\phi \sim m$ ), the reheating temperature simplifies as

$$T_{\text{reh}} \approx \left( \frac{90}{\pi^2 g_* \kappa} \Gamma_\phi^2 \right)^{1/4}. \quad (3.16)$$

Assuming a constant  $\omega_\phi$  and a thermodynamic transition. Therefore, the number of e-folds during the reheating is defined as follows

$$N_{\text{reh}} = \frac{1}{3(1 + \omega_\phi)} \ln \left( \frac{\rho_{\text{end}}}{\rho_{\text{reh}}} \right), \quad (3.17)$$

where  $\rho_{\text{end}} \sim V(\phi_{\text{end}})$  and  $\rho_{\text{reh}} = \frac{\pi^2}{30} g_* T_{\text{reh}}^4$ . Hence, we receive

$$N_{\text{reh}} = \frac{1}{3(1 + \omega_\phi)} \ln \left[ \frac{V(\phi_{\text{end}})}{\frac{\pi^2}{30} g_* T_{\text{reh}}^4} \right], \quad (3.18)$$

$$\omega_{\text{reh}} = \frac{1}{3N_{\text{reh}}} \ln \left[ \frac{V(\phi_{\text{end}})}{\frac{\pi^2}{30} g_* T_{\text{reh}}^4} \right] - 1. \quad (3.19)$$

The figures 4, 5, 6 and 7 are an analysis of these equations. For each figure, we have shown separately the range of our parameters. The reheating must occur after the end of the inflation, so the equation of state should satisfy  $-1/3 < \omega < 1$ . The plots cover  $10^5 - 10^{15}$  GeV, safely above the the lower bound of the Big-Bang Nucleosynthesis ( $\gtrsim 1$  MeV). The range of 1-60 e-folds is plausible, though the realistic scenarios typically favor  $N_{\text{reh}} \lesssim 20$ . The plots correctly show shorter reheating for stiffer  $\omega_{\text{reh}}$  at the fixed  $T_{\text{reh}}$ . Therefore, the plots are physically reasonable if  $\omega_{\text{reh}} > -1/3$  is enforced. The reheating temperatures and durations align with the theoretical expectations, and no immediate conflicts arise from the presented ranges. These results help to quantify viable reheating scenarios within the observational and thermodynamic constraints.

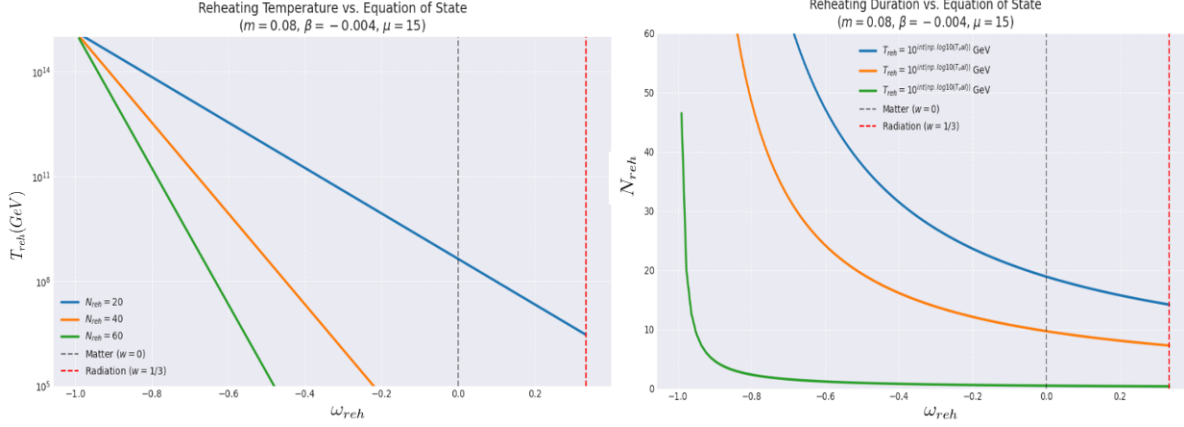


Figure 4: The left plot illustrates that how the universe’s temperature at the end of the reheating depends on the cosmic fluid’s behavior, parameterized by  $\omega_{\text{reh}}$ , which determines the expansion rate. For a fixed number of the e-folds  $N_{\text{reh}}$ , a faster expansion (higher  $\omega_{\text{reh}}$ ) dilutes the energy and induces a low temperature. The dashed lines mark the key cases:  $\omega_{\text{reh}} = 0$  (matter-like) and  $\omega_{\text{reh}} = -1/3$  (radiation-like). The right plot shows that how  $N_{\text{reh}}$  varies with  $\omega_{\text{reh}}$  for the fixed reheating temperatures. A softer equation of state ( $\omega_{\text{reh}} \rightarrow -1/3$ ) slows the energy dilution, which permits a longer reheating. A stiffer state requires the shorter reheating to achieve the same temperature. This reveals an interplay between the expansion dynamics and the thermal history post-inflation.

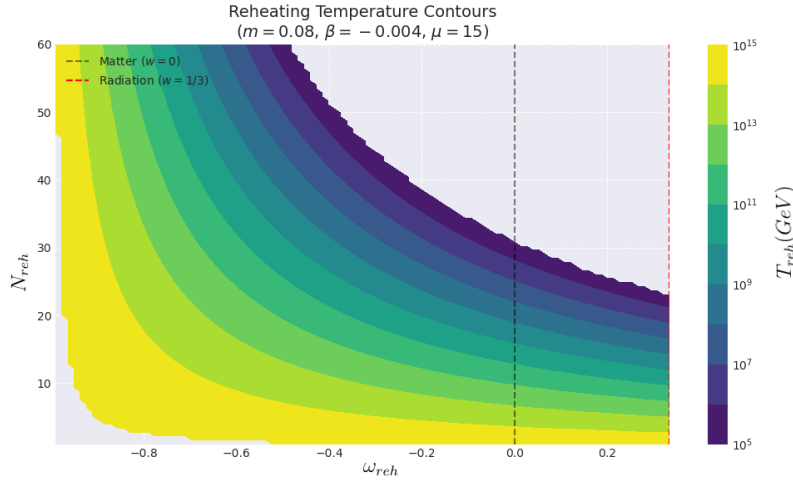


Figure 5: This contour plot provides a comprehensive visualization of the reheating temperature landscape, shaped by the effects of the reheating equation of state and the duration. Given the energy density at the end of the inflation, the temperature after the reheating sensitively depends on how the Universe expands and cools during this epoch. The regions with the higher  $\omega_{\text{reh}}$  correspond to the faster dilution of the energy density, which yield the lower reheating temperatures for the same reheating length. The interplay manifests as nonlinear contours and reflects the exponential scaling of the energy density with  $N_{\text{reh}}$  and equation of state. This reveals the physically plausible reheating scenarios, consistent with the theoretical inflation models.

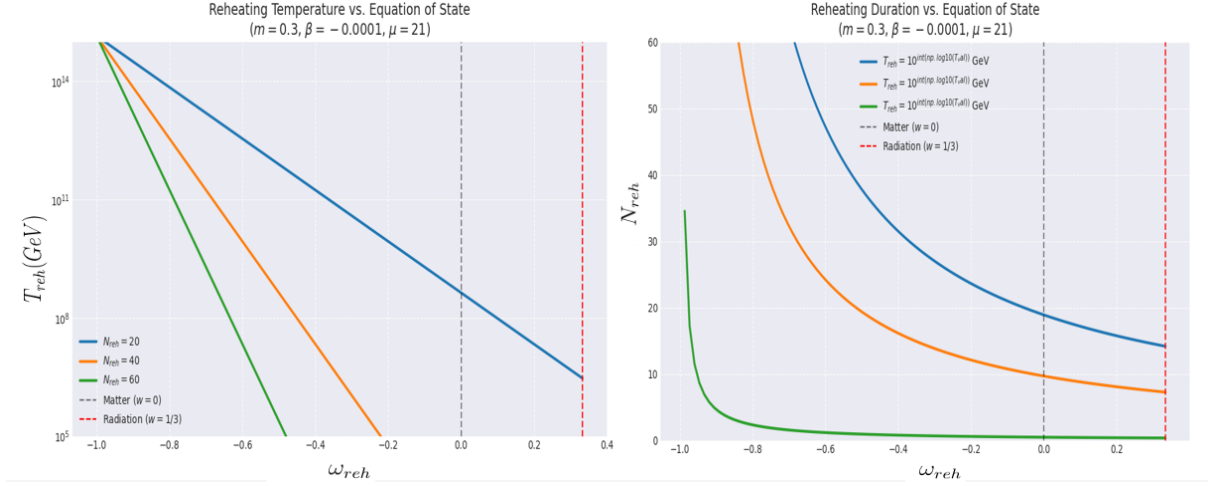


Figure 6: The left figure shows that how the reheating temperature varies with the equation of state parameter  $\omega_{\text{reh}}$ . The different durations ( $N_{\text{reh}}$ ) are fixed. A larger  $\omega_{\text{reh}}$  (with the range from  $-1$  to  $1/3$ ) means the faster energy dilution, which reduces the temperature. The key case-matter ( $\omega_{\text{reh}} = 0$ ) and the radiation domination ( $\omega_{\text{reh}} = 1/3$ ) have been highlighted. They illustrate that how the reheating dynamics shapes the early universe's thermal state. The right figure demonstrates that, for a given reheating temperature, a stiffer equation of state (higher  $\omega_{\text{reh}}$ ) requires fewer e-folds ( $N_{\text{reh}}$ ) due to rapid energy loss, while the softer equations of state need the longer reheating. The boundaries at  $\omega_{\text{reh}} = 0$  and  $1/3$  mark the standard reheating scenarios, i.e. linking the expansion behavior to the post-inflation thermal history.

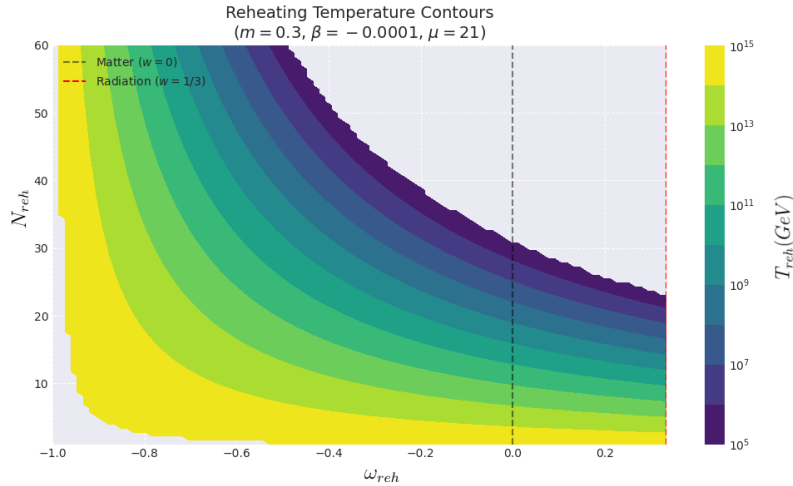


Figure 7: This contour map consolidates the dependence of the reheating temperature on both the equation of state and the reheating duration. This illustrates that the full parameter space has been spanned by  $\omega_{\text{reh}}$  and  $N_{\text{reh}}$ . The color gradation (log scale) demonstrates how the interplay between the expansion dynamics (controlled by  $\omega_{\text{reh}}$ ) and the reheating time determines the final thermal state of the Universe. The regions of the high reheating temperature correspond to the relatively short reheating epochs with the soft equations of state, whereas the cooler reheating temperatures arise for the longer reheating durations or the stiffer equations of state. This plot provides a comprehensive overview of the reheating phase, which is consistent with the specified inflationary energy scale and the model parameters.

The figures 4-7 present an analysis of two parameter sets, with the similar trends, expected for other values (not shown). Due to the wide range, selected for  $T_{\text{reh}}$ , the figures appear nearly identical. The parameters  $\beta$ ,  $m$  and  $\mu$  demonstrate comparable effects on the reheating dynamics in both cases. While the calculated reheating parameters ( $T_{\text{reh}}$ ,  $N_{\text{reh}}$  and  $\omega_{\text{reh}}$ ) show the measurable differences between the sets. Because of the broad scales using, these variations are visually subtle in the plots. Nevertheless, all graphical results remain fully consistent with the underlying reheating physics.

- **Discussion of the Limitations**

In the context of the large-field inflationary models, the slow-roll condition fails when the inflaton field value is  $\phi \lesssim m$ . This is corresponding to the inflationary phase's termination. This behavior aligns precisely with the theoretical constraints, derived from brane-antibrane separation dynamics [62]. At substantially larger field values ( $\phi \gg m$ ), the scalar potential enjoys protection through the shift symmetry, a characteristic property of the axion-like fields in the string-theoretic framework [60].

The higher-order perturbative corrections and non-perturbative effects may gain relevance when  $\phi \sim m$ . However, their contributions are naturally regulated by the intrinsic cut-off scale  $\mu$ , embedded in the functional form of  $F(\phi)$  [22]. The specific coupling structure  $f(\phi, T) = \beta F(\phi)T$  necessarily mediates direct energy transfer between the oscillating inflaton field  $\phi$  and the fundamental matter fields during the reheating epoch.

The efficiency of the reheating mechanism exhibits dual dependence on: (i) the dimensionless coupling parameter  $\beta$ , and (ii) the complete spectrum of the available inflaton decay channels. Although the potential gradient near  $\phi \sim m$  suggests an efficient energy transfer, a comprehensive treatment requires an explicit specification of the matter sector Lagrangian  $L_m$ . It should include particular couplings to the Standard Model constituents such as the Higgs field [64].

## 4 Conclusions

We included the new term  $F(\phi) T$  in the Einstein-Hilbert action, motivated by the  $f(R, T)$  gravity. We initially focused on the inflationary dynamics through the arbitrary

functionals  $F(\phi)$  and  $V(\phi)$ . Afterward, we computed the cosmological observables “ $r$ ” and “ $n_s$ ” for the special forms of  $F(\phi)$  and  $V(\phi)$ . Therefore, we produced appropriate data corresponding to the D-brane inflation. Then, we compared the accuracy and precision of our data with the experimental data.

We applied the following numerical values for the coupling constant, i.e.,  $\beta = -0.004$  and  $-0.0001$ , and the parameter “ $\mu$ ” was left as a variable to obtain “ $r$ ” and “ $n_s$ ”. All the data have been shown in the tables 1 and 2, and the paragraphs immediately after these tables. Our method covered the left-hand side of the Planck’s data, as it was depicted in the figures 2 and 3. By choosing suitable numerical values for “ $\beta$ ” and “ $\mu$ ” we can also cover the entire Planck data surface.

The figure 3 displays the results for two situations. In the first case, which was depicted by the blue color, the parameters have been selected as  $m = 0.08$ ,  $\beta = -0.004$  and  $15 \leq \mu \leq 50$ . As a result, the data remain in the designated region of the Planck data in the  $(n_s, r)$ -space plot as blue. In the second case, the parameters for the pink part are  $m = 0.3$ ,  $\beta = -0.0001$  and  $7 \leq \mu \leq 21$ . The pink points in the  $(n_s, r)$ -space stay in the  $2\sigma$  region. By choosing some specific values for the parameter “ $\mu$ ” from the range  $3 \leq \mu \leq 100$ , we can cover the left-hand side of the Planck data. Typically, if we choose a wider range for the parameters “ $\beta$ ” and “ $\mu$ ”, we can completely cover all the sweet spots of the Planck data.

We compared our results with the standard simplest D-brane inflation in the Einstein’s gravity. As it is clear in the figure 3, our results completely agree with the Planck data. The case  $\beta = 0$  elaborates the identical results with the standard simplest D-brane inflation in the Einstein’s gravity.

We comprehensively analyzed the dynamics of the reheating phase via the four figures 4 - 7. The presented results in these figures are fully consistent with both our theoretical interpretation of the reheating and the underlying equations that describe this epoch. The graphical representations directly reflected the physical behavior, derived from our computations. They are completely consistent with the coherent correspondence between the analytical predictions and the numerical results.

## References

- [1] A. H. Guth, Phys. Rev. **D 23** (1981) 347.
- [2] A.D. Linde, Inflationary Cosmology, Phys. Lett. **B 108** (1982) 389.
- [3] A. A. Starobinsky, Phys. Lett. **B 91** (1980) 99.
- [4] A. Albrecht and P.J. Steinhardt, Phys. Rev. Lett. **48** (1982) 1220.
- [5] D. H. Lyth and A. Riotto, Phys. Rept. **314** (1999) 1.
- [6] A. R. Liddle and D. H. Lyth, “*Cosmological inflation and large-scale structure*”, Cambridge University Press, UK (2000).
- [7] BICEP, Keck collaboration, Phys. Rev. Lett. **127** (2021) 151301.
- [8] Planck Collaboration, “*Planck 2018 results. VI. Cosmological parameters*”, A&A 641, A6 (2020), [arXiv:1807.06209 [astro-ph.CO]].
- [9] Planck Collaboration, “*Planck 2013 results. XVI. Cosmological parameters*”, A&A 571, A16 (2014), [arXiv:1303.5076 [astro-ph.CO]].
- [10] L. Boubekeur and D. Lyth, JCAP **07** (2005) 010.
- [11] R. Kallosh, A. D. Linde, JCAP **09** (2019) 030.
- [12] C. M. Lin, JCAP **06** (2020) 015.
- [13] K. Kohri, C. M. Lin and D. H. Lyth, JCAP **12** (2007) 004.
- [14] K. Dimopoulos, Phys. Lett. **B 809** (2020) 135688.
- [15] G. German, JCAP **02** (2021) 034.
- [16] J. Martin, C. Ringeval and V. Vennin, Phys. Dark Univ. **5-6** (2014) 75-235.
- [17] J. Hoffmann, D. Sloan, Phys. Rev. **D 104** (2021) 123542.
- [18] K. A. Olive, Phys. Rept. **190** (1990) 307-403.

- [19] M. Tegmark et al. [SDSS Collaboration], “*Cosmological parameters from SDSS and WMAP*”, Phys. Rev. **D 69** (2004) 103501 [astro-ph/0310723].
- [20] J. Polchinski, Phys. Rev. Lett. **75** (1995) 4727.
- [21] S. Kachru, R. Kallosh, A. D. Linde, et al. JCAP **0310** (2003) 013; G. Dvali, Q. Shafi and S. Solganik, Phys. Lett. **B 450** (2001) 72-82.
- [22] C. P. Burgess, M. Majumdar, D. Nolte, F. Quevedo, G. Rajesh and R. J. Zhang, JHEP **07** (2001) 047.
- [23] J. Garcia-Bellido, R. Rabadan and F. Zamora, JHEP **01** (2002) 036.
- [24] J. Martin, C. Ringeval and V. Vennin, Phys. Dark Univ. **5-6** (2014) 75-235.
- [25] R. Kallosh, A. Linde and Y. Yamada, JHEP **01** (2019) 008.
- [26] R. Kallosh, A. D. Linde, and A. Roest, JHEP **198** (2013)1311.
- [27] J. J. M. Carrasco, R. Kallosh and A. Linde, JHEP **10** (2015) 147.
- [28] R. Kallosh and A. Linde, Phys. Rev. **D 91** (2015) 083528.
- [29] R. Kallosh and A. Linde, Phys. Lett. **B 798** (2019) 134970.
- [30] M. Galante, R. Kallosh, A. Linde and D. Roest, Phys. Rev. Lett. **114** (2015) 141302.
- [31] Planck Collaboration, “*Planck 2018 results. X. Constraints on inflation*”, A&A 641, A10 (2020), [arXiv:1807.06211 [astro-ph.CO]].
- [32] A. D. Linde, Phys. Lett. **B 129** (1983) 177.
- [33] K. Freese, J. A. Frieman and A. V. Olinto, Phys. Rev. Lett. **65** (1990) 3233.
- [34] F. C. Adams, J. R. Bond, K. Freese, J. A. Frieman and A. V. Olinto, Phys. Rev. **D 47** (1993) 426.
- [35] A. A. Starobinsky, Phys. Lett. **B 91** (1980) 99.
- [36] V. R. Ivanov, S. V. Ketov, E. O. Pozdeeva and S. Yu. Vernov, JCAP **03** (2022) 058.

- [37] A. Goncharov and A. D. Linde, Sov. Phys. JETP **59** (1984) 930; G. Dvali and S.H. Tye, Phys. Lett. **B 450** (1999) 72-82.
- [38] E. E. Flanagan, Phys. Rev. Lett **92** (2004) 07110.
- [39] M. Ferraris, M. Francaviglia and I. Volovich. Class. Quant. Grav. **11** (1994) 1505-1517.
- [40] G. R. Bengochea and R. Ferraro, Phys. Rev. **D 79** (2009) 124019; S. Teymourashlou and D. Kamani, Eur. Phys. J. **C 81** (2021) 761, arXiv:2108.10164 [hep-th].
- [41] S. Nojiri and S. D. Odintsov, Phys. Lett. **B 631** (2005) 1-6.
- [42] T. Harko, F. S. N. Lobo, S. Nojiri and S. D. Odintsov, Phys. Rev. **D 84** (2011) 024020.
- [43] R. Ferraro and F. Fiorini, Phys. Rev. **D 75** (2007) 084031.
- [44] S. Nojiri and S. D. Odintsov, Phys. Lett. **B 599** (2004) 173.
- [45] G. Allemandi, A. Borowiec, M. Francaviglia and S.D. Odintsov, Phys. Rev. **D 72** (2005) 063505; H. Daniali and D. Kamani, Nucl. Phys. **B 975** (2022) 115683, arXiv:2202.09347 [hep-th].
- [46] O. Bertolami, C. G. Boehmer, T. Harko and F.S.N. Lobo, Phys. Rev. **D 75** (2007) 104016.
- [47] P. Rudra, K. Giri. Nucl. Phys. **B 967** (2021) 115428; D. Kamani, Phys. Lett. **B 564** (2003) 123-131, arXiv:hep-th/0304236.
- [48] X. Zhang, C. Y. Chen and Y. Reyimuaji. Phys. Rev. **D 105** (2022) 043514.
- [49] V. Dzhunushaliev, V. Folomeev, B. Kleihaus, and J. Kunz. Eur. Phys. J. **C 74** (2014) 1.
- [50] C. Y. Chen and Y. H. Kung. Phys. Dark Univ. **35** (2022) 100956.
- [51] X. Liu, T. Harko, and S. D. Liang. Eur. Phys. J. **C 76** (2016) 1.

- [52] J. Rubio and C. Wetterich. Phys. Rev. **D 96** (2017) 063509.
- [53] A. Belhaj, M. Benali, Y. Hassouni, and M. Lamaaoune. Int. J. Mod. Phys. **A 38** (2023) 2350043.
- [54] M. Gamonal. Phys. Dark Univ. **31** (2021) 100768.
- [55] P. A. R. Ade et al. [Planck], Astron. Astrophys. **571** (2014) A22.
- [56] Ade, Peter AR, et al. “*Improved constraints on primordial gravitational waves using Planck, WMAP, and BICEP/Keck observations through the 2018 observing season*”, Phys. Rev. Lett. **127**. 15 (2021), 151301.
- [57] D. S. Salopek, J. R. Bond and J. M. Bardeen. Phys. Rev. **D 40** (1989) 1753.
- [58] M. Cicoli, C. P. Burgess and F. Quevedo. JCAP **0903** (2009) 013.
- [59] S.B Giddings, S. Kachru and J. Polchinski, Phys. Rev. **D 66** (2002) 106006.
- [60] E. Silverstein and D. Tong, Phys. Rev. **D 70** (2004) 103505.
- [61] C. P Burgess, JHEP **07** (2007) 047.
- [62] S. Kachru et al. Phys. Rev. **D 68** (2003) 046005.
- [63] I. R. Klebanov and M. J. Strassler, JHEP**08** (2000) 052.
- [64] Kofman et al. Phys. Rev. **D 56** (1997) 3258.